buildings

MDPI

Article

Experimental and Numerical Investigation of Geosynthetic-Reinforced Pile-Supported Embankments for Loose Sandy Soils

Rashad Alsirawan *, Ammar Alnmr and Edina Koch

Department of Structural and Geotechnical Engineering, Széchenyi István University, 9026 Gyor, Hungary; alnmr.ammar@hallgato.sze.hu (A.A.); koche@sze.hu (E.K.)
* Correspondence: alsirawan.rashad@sze.hu

Abstract: This research focuses on advancing the geosynthetic-reinforced pile-supported embankment technology over loose sandy soil. A small-scale laboratory model supported by floating piles and a geotextile layer was constructed, and a numerical model was validated against laboratory measurements. This study aims to achieve a more uniform distribution of the load over all piles of the system via a parametric study that analyzes the influence of embankment fill material, horizontal reinforcement scenarios, pile cap shape, and pile type. The results demonstrate that using embankment fill with high cohesion and internal friction properties leads to a significant reduction of 46% and 37% in maximum settlements, respectively, and similarly, results in a noteworthy reduction of 48% and 50% in differential settlements. The incorporation of two geotextile layers contributes to a reduction of up to 30% in maximum settlement. The utilization of plus-shaped caps in small areas, with an area equal to three times the cross-sectional area of the pile, has been substantiated as the preeminent approach for the reduction of settlements. Piles with caps also present better behavior regarding differential settlements compared to longer piles and piles with bigger diameters under the same volume condition.

Keywords: small-scale laboratory model; uniform load distribution; parametric study; geosynthetic-reinforced pile-supported embankments

check for updates

Citation: Alsirawan, R.; Alnmr, A.; Koch, E. Experimental and Numerical Investigation of Geosynthetic-Reinforced Pile-Supported Embankments for Loose Sandy Soils. *Buildings* **2023**, *13*, 2179. https://doi.org/10.3390/buildings13092179

Academic Editors: Marian Drusa, Jaroslaw Rybak and Andrea Segalini

Received: 7 August 2023
Revised: 18 August 2023
Accepted: 25 August 2023
Published: 28 August 2023

Copyright: © 2023 by the authors. Licensee MDPI, Basel, Switzerland. This article is an open access article distributed under the terms and conditions of the Creative Commons Attribution (CC BY) license (https://creativecommons.org/licenses/by/4.0/).

1. Introduction

In the world of modern construction, geosynthetics have become a crucial factor in promoting the development of sustainable soil foundations reinforced with these materials. This reinforcement greatly improves the load-bearing capacity while also reducing the risk of harmful settlement problems [1,2]. Geosynthetic-reinforced pile-supported embankments (GRPS) offer a more developed alternative to support heavy loads. These structures involve the use of geosynthetics, such as geotextiles or geogrids, to reinforce the soil and the piles to transfer the load to deep layers of stiff soil or rock. The combination of these two elements allows for the construction of stable and durable embankments on sites with weak or compromised soil conditions [3].

The significance of geosynthetic-reinforced piled embankments stands out prominently in practical applications, such as constructing buildings, tanks, walls, and embankments to elevate the foundations of highway and railway. These innovative solutions offer a means to overcome the challenges posed by unstable soil conditions and excessive settlement, thereby ensuring the stability, durability, and long-term performance of structures and crucial transportation infrastructure. The primary mechanisms of GRPS embankments involve the effect of the tensioned membrane and soil arching. Soil arching arises due to differential movement between the piles and underlying soil, creating shear stress that transfers vertical loads to the piles while reducing vertical stress on the soil between the piles. The tensioned membrane effect arises from the geosynthetic between

the piles, which lowers the vertical stress on the soil below. In contrast, the installation of a rigid platform above the subsoil and piles eliminates the effect of the soil-arching tensioned membrane. However, stress concentration still occurs on the piles due to their differing modulus compared to the soil [4].

Previous design methods for GRPS embankments have mainly concentrated on their application on soft soil foundations, often overlooking the behavior concerning different soil types. These methods have been proposed by researchers such as Hewlett and Randolph [5], Kempfert et al. [6], Abusharar et al. [7], BS 8006 [8], EBGEO [9], Van Eekelen et al. [10], Pham [11], and Alsirawan et al. [12].

Historically, researchers have conducted a variety of studies aimed at gaining a deeper comprehension of the influence of fill properties on the behavior of GRPS embankments over soft soils. Nuñez et al. [13] employed well-graded gravelly sand, along with sand that had been treated with silt and cement, as the fill material for the embankment. Upon close examination, it was evident that the utilization of treated soil led to a remarkable increase of more than 85% in load efficiency. Chevalier et al. [14] utilized a combination of numerical and discrete element methods; the finding indicates that the friction angle of embankment fill soil contributes to improved load efficiency of the piles. In a study by Van Eekelen et al. [15], a series of experiments were carried out employing granular fill ($\varphi = 49^{\circ}$) and sand fill ($\varphi = 40.88^{\circ}$) materials; φ is the angle of internal friction. The research revealed that fill with an elevated internal friction angle (granular) fosters soil arching during subsoil consolidation, leading to improved load efficiency. Additionally, this contributes to the reduction of tension within the geosynthetic reinforcement. Xu et al. [16] conducted many laboratory experiments to examine the influence of cohesion of embankment fill through the addition of fiber to sand, finding that this resulted in improved load efficiency and reduced subsoil settlement. Three-dimensional numerical analysis was conducted by Pham and Dias [17], and the results confirmed the positive influence of embankment soil cohesion on the load efficiency and on the differential settlements.

Briançon and Simon [18] conducted a comparative analysis between the behavior of a full-scale model of a GRPS embankment and that of a capped-piled embankment. The results indicated that, when employing two geogrid layers, the load efficiency of the GRPS embankment showed a minor decrease in comparison to the load efficiency of the capped-piled embankment under similar conditions. Through a set of laboratory experiments, Van Eekelen et al. [15] discovered that using two layers of geogrid, rather than just one, leads to a slight improvement in soil arching and an increase in load efficiency, in particular when the first layer is placed directly above the piles. Additionally, the study found that the impact of using geotextile or geogrid on the performance is insignificant. These conclusions were supported by the research of Kerry Rowe and Liu [19]. Pham et al. [20] executed a three-dimensional numerical modeling of GRPS embankments. The results of the numerical analysis additionally demonstrate that the geosynthetic, operating via its tensioned-membrane effect, assumes a critical function in enhancing the load transmission to the piles. The inclusion of geosynthetic materials leads to a mitigation of differential settlements and a decrease in the likelihood of soil yielding above the pile heads. Through a 3D numerical analysis of GRPS embankment, Alsirawan and Koch [21] found that the positioning of geosynthetic layers significantly affects the behavior of the GRPS embankment, and the use of two layers of geogrid has a minor impact on load efficiency. Hello and Villard [22] conducted a numerical study that integrated discrete and finite methods, which revealed that larger pile cap sizes are associated with higher load efficiency and reduced geotextile displacements. Zhang et al. [23] studied the impact of cap shape and pattern on maximum strains experienced by geosynthetic reinforcements. Their numerical analysis revealed that these factors significantly affect the maximum strains in geosynthetic materials. Wang et al. [24] conducted five experimental tests on GRPS embankment, and the results revealed that the pile cap size and pile spacing play a crucial role in determining the load efficiency, while the stiffness of the geogrid had a comparatively lesser impact. In their study, Alsirawan and Koch [21] examined the influence of varying the cover ratio,

which is defined as the proportion of the cross-sectional area of piles to the area of the load transfer platform, by enlarging the pile cap area and the pile cross-sectional area on the load efficiency of GRPS embankments. The findings revealed that increasing the cap area resulted in higher load efficiency, while increasing the pile cross-sectional area led to a decrease in load efficiency.

The available research on floating piles in GRPS embankments over soft soil is considered limited. However, this solution has been found to be effective and preferable, particularly when dealing with substantial thicknesses of subsoil layers. It is worth noting that BS8006 [8] is currently the only standard that takes into consideration the pile type, whether end-bearing or floating, in the design of GRPS embankments.

To assess the effectiveness of soil–cement columns with a floating configuration, Pongsivasathit et al. [25] conducted large-scale model experiments. Their findings led to the conclusion that employing floating piles represents a cost-effective and viable solution for the thick layers of soft soils. To better comprehend the behavior of an embankment supported by geogrid reinforcement and floating piles, a field experiment was performed by Cao et al. [26]. The findings indicate that the downward movement of the floating piles allowed for the load of the embankment fill to be transferred from the piles to the subsoil. The results indicate a reduction of tensioned membrane effects, soil-arching effects, strains in the geogrid, and stress concentration ratios. In their small-scale model tests, Xu et al. [16] studied the mechanism in which loads are transferred in embankments supported by floating piles. The researchers found that when end-bearing or floating piles are used, the load efficiency of the pile increases with the construction of embankment. However, they also observed that when the floating piles begin to penetrate the underlying soil under a heavy load, the load efficiency of the piles decreases as the embankment and surcharge load increase. Zhang et al. [27] constructed a small-scale model to compare the behavior of both floating piles and end-bearing piles. Their findings indicate that the stress concentration ratio under end-bearing piles is higher than that under floating piles and increases with larger pile spacing, and the floating piles contribute in decreasing the differential settlements relative to the end-bearing piles. In a sequence of three centrifuge model experiments, Shen et al. [28] discovered that in cases where end-bearing piles were employed, differential settlement occurred at the embankment base, leading to the predominant transfer of the embankment load to the piles. Conversely, floating piles exhibited characteristics akin to rigid inclusions, effectively creating a composite foundation with the surrounding soil. Furthermore, their findings highlighted that the utilization of end-bearing piles possessing a lower modulus contributes to a discernible elevation in both the total and differential settlement of subsoil and piles at the embankment base.

The use of GRPS embankment on sand foundations has received relatively limited attention in the literature, with only a handful of studies exploring this topic. Xu et al. [16] performed six tests of a scaled model of GRPS embankment over sandy soil to examine the influence of embankment fill cohesion, pile type (floating or end-bearing), and pile (cap) spacing on the GRPS embankment performance. The study produced the following findings: the cohesion of embankment fill contributes in increasing the load efficiency of the pile and in decreasing the settlement of the subsoil. Both floating piles and end-bearing piles can be utilized to provide support for the GRPS embankment, with the latter exhibiting less soil arching but leading to higher maximum settlement compared to end-bearing piles. The formation of soil arch starts when the ratio of the height of the embankment to clear distance between piles (caps) falls within the range of 0.5 to 0.7. Esmaeili and Khajehei [29] performed a laboratory model to examine the impact of the deep mixed pile on the bearing capacity and the settlements of an embankment over loose sandy soil, the results show that the distribution of piles in triangle and square patterns contributes in increasing the bearing capacity by 63.7% and 63%, respectively. Furthermore, in both patterns, the center piles bear the vertical load and reduce the settlement while the side and mid piles resist the horizontal loads and soil sliding. The measured load efficiency of the center piles exceeds 50% in both patterns.

Given the limited exploration into the implementation of GRPS embankments on loose sand foundations, specifically focusing on aspects such as pile configurations, pile types, embankment soil cohesion, and pile spacing, there exists a pertinent gap that necessitates deeper inquiry. It becomes imperative to delve more extensively into this subject, broadening the comprehension of how GRPS embankments interact with this particular foundation soil type. Such investigation is pivotal not only for a more comprehensive understanding of their behavior but also to uncover potential modifications that could optimize their design and construction. This study includes a small-scale model of a GRPS embankment over loose sandy soil constructed in the laboratory of Széchenyi Istvan university as a first step, to be followed by numerical analysis using Plaxis 3D software. Improving the performance of this technology in loose sandy soil through parametric study includes the influence of embankment fill properties, different scenarios of horizontal reinforcement, the shape of pile cap for the same area, and the shape of the pile for the same pile volume on the load efficiency of pile and settlements of the embankment.

The study began by constructing a small-scale model of a GRPS embankment over loose sandy soil in the laboratory of Széchenyi Istvan University. This is followed by a numerical analysis using Plaxis 3D software. The aim is to improve the technology's performance in loose sandy soil. This involves testing various factors, such as embankment fill properties, different horizontal reinforcement scenarios, diverse pile cap shapes while maintaining the same area, and varied pile shapes while keeping the pile volume constant. The focus is on how these factors affect the pile's load efficiency and the settlement of the embankment.

2. Model Tests

2.1. Test Setup

The experimental setup for a small-scale GRPS embankment subjected to a vertical load is depicted in Figure 1. The test box, which was constructed using reinforced steel and tempered glass, had dimensions of 1.5 m in length, 0.2 m in width, and 1.0 m in height. The GRPS embankment, equipped with floating piles, is displayed from a vertical cross section in Figure 1a. Meanwhile, Figure 1b offers a cross-sectional illustration of the GRPS embankment at its base, showcasing 16.

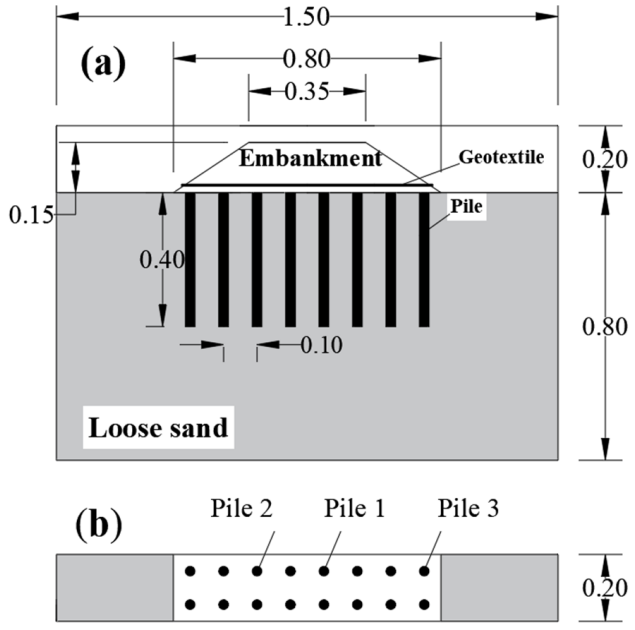


Figure 1. (**a**) Vertical cross section, (**b**) cross section at embankment base-dimensions in meters.

2.2. Properties of Used Materials

For the subsoil foundation, sandy soil was utilized, and the laboratory tests revealed a uniformity coefficient of 2.23 and a curvature coefficient of 0.96 for the soil (D_{10} = 0.13 mm, D_{60} = 0.29 mm, D_{30} = 0.19 mm). As a result, the sand is categorized as poorly graded sand (SaP) based on the EN ISO 14688-1 [30]. This sand was brought from the Danube bank in Hungary. The process of determining the relative density of sand involved the use of the sand-raining technique, which utilized a bucket equipped with a tube of 3.5 cm in diameter and a tap. The sand was poured into a cylindrical mold with dimensions of 151 mm in diameter and 114 mm in height in a controlled manner to ensure an even placement and proportionate distribution of soil according to the desired relative density. To achieve a relative density of 30% for the sandy soil, multiple trials were conducted to adjust the height of the sand flow and the speed of the sand particles. A tap diameter of 10.0 mm and a falling height of 200 mm were used in the experiment to attain the desired relative density. The maximum γ_{dmax} and minimum γ_{dmin} dry unit weights of the sand were established according to the (EN ISO 14688-1) [30] standard, with values of 17.03 and 14.53 kN/m^3, respectively. In order to assess the characteristics of the sandy soil, a series of five direct shear tests, three triaxial tests, and three oedometric tests were carried out; the findings obtained from these tests are documented in Table 1. The embankment was constructed using gravelly soil with a uniformity coefficient of 11.1 and a curvature coefficient of 0.198 (D_{10} = 0.27 mm, D_{60} = 3 mm, D_{30} = 0.4 mm), which classified it as medium-graded gravel (GrM), EN ISO 14688-1 [30]. The gradation of both the sandy and the gravelly soils can be seen in Figure 2. The results of the Standard Proctor compaction tests indicated that the gravelly soil had a dry density of 18 kN/m^3, with a compaction degree of 89% and an optimum water content of 5.3%. Four triaxial tests were conducted to evaluate the mechanical properties of the embankment soil, and the relevant data are presented in Table 1.

Table 1. Summary of soil properties.

Basic Parameters	Characters and Units	Embankment Soil	Sandy Soil
Dry unit weight	γ_d (kN/m^3)	18.0	15.2
Angle of internal friction	φ°	35.0	25.2
Dilatancy angle	Ψ°	5.0	0.0
Cohesion	c (kPa)	2.0	0.0
Secant modulus	E_{50}(kN/m^2)	43,830	17,220
Oedometric modulus	E_{oed} (kN/m^2)	-	15,120
Unloading/reloading modulus	E_{ur} (kN/m^2)	155,250	56,825
Stiffness moduli correspond to confining pressure of 100 kPa.			

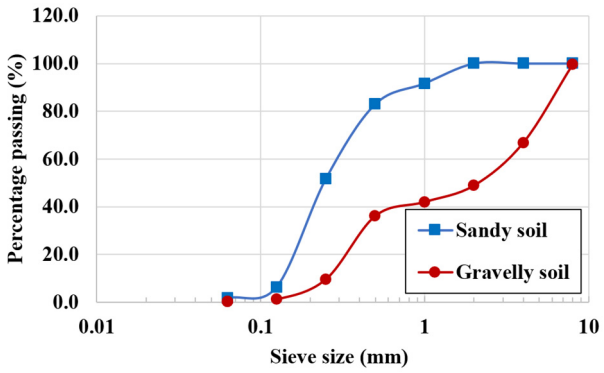


Figure 2. Particle size distribution curve of sandy and gravelly soils.

The type of the geosynthetic utilized in this study is composed of polyethylene material, and it has a thickness of 4.2 mm. The product features an aperture size of 18 × 11 mm and has a mass of 0.120 kg/m^2. To determine its mechanical properties, a tensile test was conducted in the laboratory. The results showed that the transverse and longitudinal tensile stiffness of the geotextile were approximately 47.5 kN/m and 34.0 kN/m, respectively. The piles were fabricated from epoxy material obtained from the IPox Chemicals Company located in Budapest. The dimensions of the piles used in this study were 27.0 mm in diameter and 400 mm in length. The unit weight of the piles was determined to be 11.8 kN/m^3, while the stiffness modulus was measured to be 5.7 GPa

2.3. A Small-Scale Model Construction

In this study, floating piles were constructed using a specific method. The construction process involved using plastic tubes, which were coated on the interior surface with a very thin layer of melted wax. After allowing the wax to dry, an epoxy material was poured into the tube and left to cure for 48 h. Finally, the tube was slightly heated to melt the wax and enable the extraction of the epoxy pile.

The construction process began by placing a 400 mm thick layer of sandy foundation using a bucket equipped with a tube and a tap. Then, 16 floating piles were installed, and the surrounding sandy soil was placed in the same manner. The resulting state after pile installation and sand placement is shown in Figure 3a. The embankment was subsequently constructed in three phases, with a total height of 150 mm. Each layer was 50 mm thick, and a single layer of geotextile was inserted during the first stage, positioned 10 mm above the pile heads. A small laboratory-manufactured roller was used to achieve the desired compaction level. To load the embankment, a hydraulic jack was utilized, which exerted load on a 34 mm × 195 mm × 17 mm steel plate. Figure 3b depicts the embankment body and the loading system.



(**a**) (**b**)

Figure 3. (**a**) Piles layout, (**b**) embankment body and loading system.

2.4. Instrumentation

Six strain gauges (type KFC-5-D16-11) were carefully installed inside two epoxy piles located close to the centerline (pile 1) and toe (pile 3) of the embankment; the cables of these sensors are illustrated in Figure 3a. Three strain gauges were installed in each pile at different levels. The installation process was meticulously conducted to ensure that the strain gauges are installed properly and that they provide accurate measurements. These sensors were connected to the laboratory computer.

To measure the maximum settlement at the embankment surface, four LVDT sensors were installed at the corners of the loading plate, as illustrated in Figure 3b. These sensors transmitted data to the laboratory computer, which calculated the average maximum settlement at the embankment surface. A total of ten sensors were employed in this test.

2.5. Loading System and Test Procedures

The test setup consisted of a hydraulic jack, a loading frame, and a control unit utilized to apply the incremental loads on the small-scale GRPS embankment model. The loads were applied manually using the hydraulic jack, starting with two steps of 0.5 kN and followed by seven increments of an average of 1 kN force each. Figure 4 shows the steps of loading. Each load increment was maintained for at least 22 min to allow sand particles to settle and reach stability. During each load increment, the average maximum settlement of the embankment surface was recorded using data from the four LVDT sensors. Meanwhile, the output of each strain gauge in millivolts per volt (mV/V) was recorded. Following the laboratory test of the small-scale model, a separate pile calibration procedure was performed, and the resulting calibration curve was used to convert the mV/V output of the strain gauges to the corresponding axial force values at each level of the strain gauges.

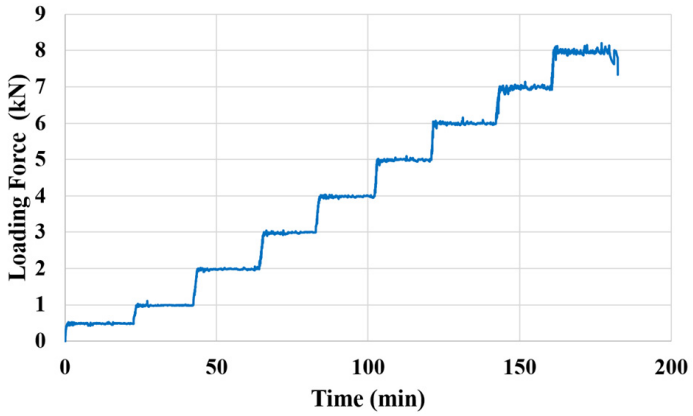


Figure 4. Loading steps during the test.

2.6. Limitations and Considerations of the Study in a Scaled Lab Model

The study conducted in a scaled laboratory model may have some limitations and considerations to keep in mind when interpreting the results. These include:

- The GRPS embankment model used in the experiment was scaled down to 1/10 of a typical field embankment size, including the embankment, piles, and spacing between piles. The tensile stiffness and strength of the geogrid were also reduced by a factor of 1/10. Furthermore, the area and force were scaled down by a factor of 1/100 to maintain proportional similarity with the original model [16].
- The experiment was conducted over a period of three days, which may have limited the study's ability to fully capture potential long-term effects, such as the creep behavior of the geotextile.
- Load transfer to the piles may be influenced by friction between the side walls of the embankment and the soil. However, the embankment in the study was relatively small in height (150 mm), and a polytetrafluoroethylene (PTFE) material was used to

minimize friction between the soil and the box walls. Therefore, any impact from side wall friction is expected to be negligible. Nonetheless, it is important to consider these limitations when interpreting the results of the study.

3. Model Simulation

With the advancement of computer technology and the increase of processing speeds for complex calculations, numerical modeling has become a more accessible and efficient means for calibrating models for use in complicated geotechnical problems [12]. By leveraging the advantages of the finite element method, this study aimed to analyze the behavior of a GRPS embankment and overcome the challenges associated with cost and implementation. To this end, a three-dimensional model was created to simulate a supported embankment over loose sandy soil. The Plaxis 3D software was utilized for the simulation and analysis of the embankment behavior. Figure 5 demonstrates the FE mesh of a small-scale model of GRPS embankment.

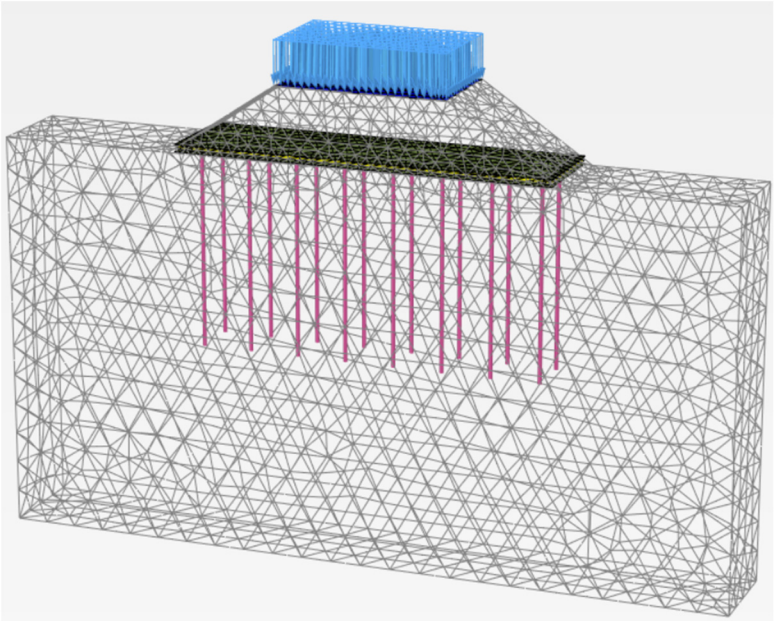


Figure 5. FE mesh of GRPS embankment over loose sand.

In the three-dimensional model, boundary conditions were imposed to ensure an accurate simulation of the embankment behavior over loose sandy soil. The bottom of the model was constrained vertically and horizontally, while the vertical boundaries were fixed in a horizontal direction. A mesh sensitivity analysis was conducted to ascertain the proper mesh size for the simulation. The results indicated that a fine mesh distribution was optimal since the settlement behavior was consistent in both very fine and fine mesh distributions. Consequently, a fine mesh consisting of 10-node triangular elements with an average size of 56 mm was created, resulting in a total of 10,503 elements, as shown in Figure 6a. In this study, a numerical analysis was conducted to simulate the behavior of the embankment fill and loose sandy soil. Initially, the Hardening Soil (HS) model was employed to simulate both layers; however, the simulation results did not match the measurements accurately. Therefore, to improve the precision of the simulation, Mohr–Coulomb (MC) and Hardening Soil (HS) models were utilized to simulate the embankment fill and sandy soil, respectively. The piles were modeled using embedded beam elements, while the geogrid was represented using elastoplastic material.

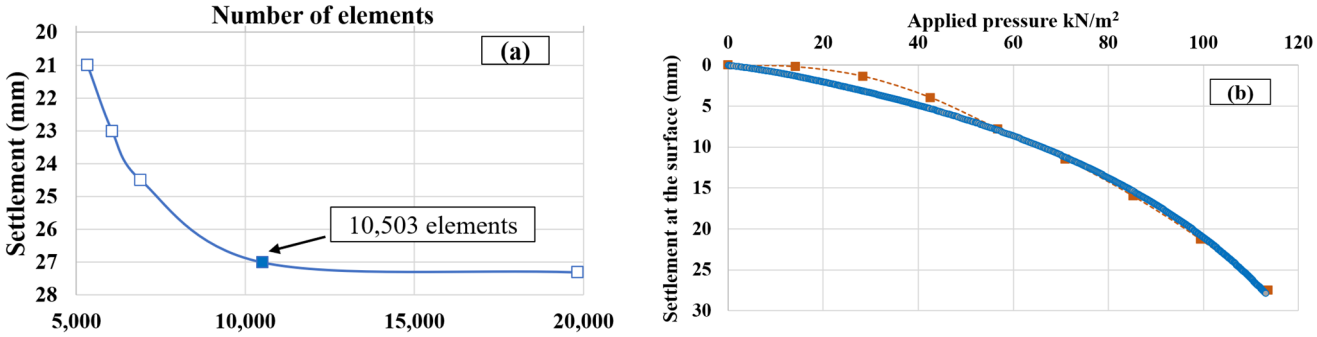


Figure 6. (**a**) The mesh sensitivity analysis. (**b**) Measured settlements vs. predicted settlement.

To verify the accuracy of the simulation, an assessment was carried out by comparing the average of the maximum settlements observed at the embankment in the laboratory. Four LVDT sensors, which yielded highly similar settlement values, were fixed on a steel plate located at the embankment surface. Then, these measurements were compared to the predicted settlement values obtained from the numerical model at the mid-point of the embankment surface. Figure 6b illustrates that the settlements from the FE analysis closely matched that of those obtained from the laboratory, indicating a high level of consistency between the two datasets.

The measured and the calculated axial forces of piles 1 and 3 were compared at two-step loading increments (2 kN, 4 kN, 6 kN, and 8 kN) following the pile calibration process. The comparison, shown in Figure 7, indicated a high level of concurrence between the predicted and measured values. The tension behavior observed in pile 3 under the embankment toe, as evident from the axial force values recorded after each loading increment, can be attributed to the pile's location, which receives horizontal forces that escalate with increasing embankment loads. This affects the axial force behavior, as shown in Figure 7b.

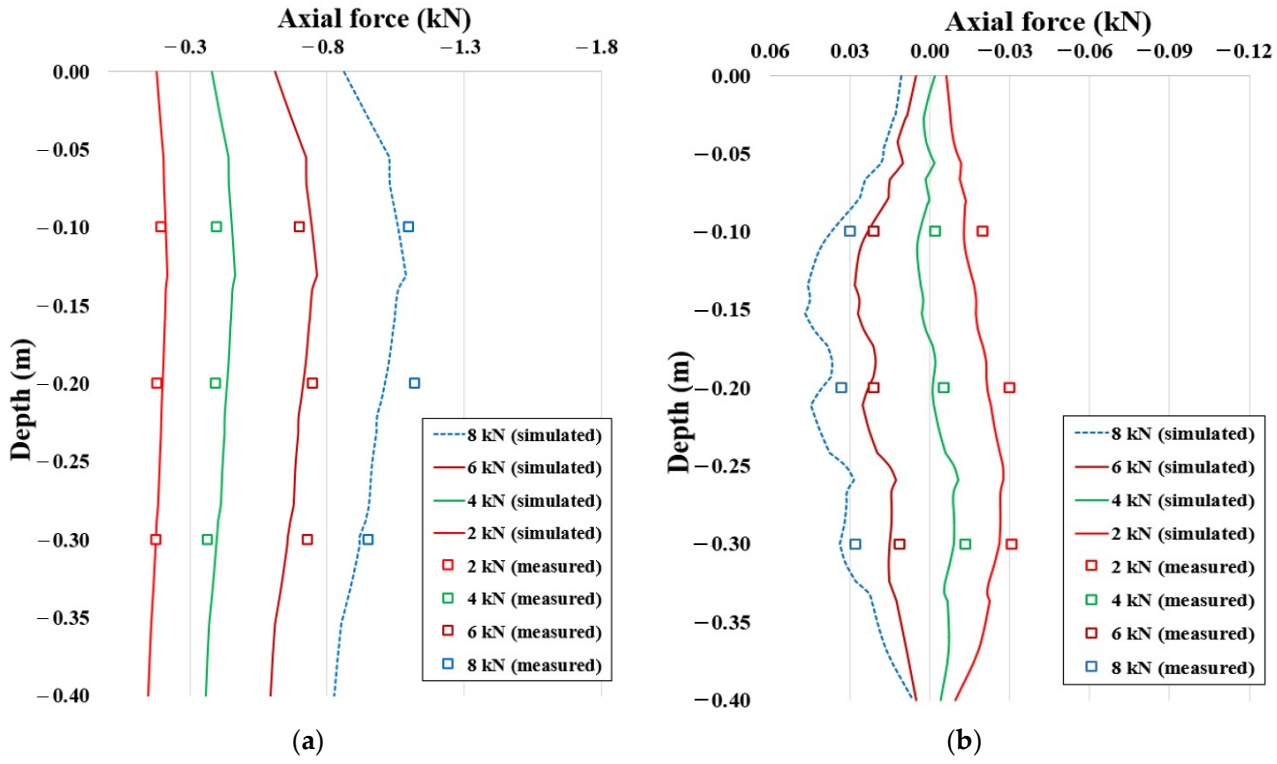


Figure 7. Comparison of measured and predicted axil forces along (**a**) pile 1 (**b**) pile 3.

4. Results and Discussion

The use of piles with geosynthetic layers as a foundation for embankments over layer(s) of soft soil is a firmly established technology. In this section, a numerical analysis was performed to examine the behavior of GRPS embankments constructed on loose sandy soil, aiming to go beyond the limitations of physical testing. The study aims to understand the mechanism of load transfer and settlement behavior in greater depth by examining a range of factors that are believed to have an impact. These factors encompass the embankment fill properties, the different scenarios of horizontal reinforcement, the shape of the pile cap for the same area, and the shape of the pile for the same pile volume.

The physical testing of GRPS embankments on loose sandy soil revealed that the significant portion of the vertical load is transmitted to the piles near the centerline of the embankment, while the remaining piles in the middle and on the sides function primarily to prevent soil sliding and to resist horizontal loading. This observation is consistent with previous research findings by Esmaeili and Khajehei [29]. This study aims to investigate modifications to this technology in order to achieve a more uniform distribution of the vertical load over the piles, with the goal of reducing settlements when used on sandy soil.

4.1. Influence of Embankment Fill Properties (φ,c,E)

Figure 8 depicts the relationship between the cohesion and the internal friction angle of the embankment fill and load efficiency of piles 1 and 2 under the final load of 8 kN, where the reference case represents the laboratory test. The results indicate that an increase in the cohesion and the internal friction angle results in a corresponding increase in the load efficiency of pile 2. It is worth noting that the internal friction angle is particularly effective in soils with low cohesion. Conversely, the load efficiency of pile 1 reduces gradually with the increase of the strength soil properties (φ,c). This phenomenon is attributed to the further and more even distribution of the applied load rather than being concentrated on the piles closest to the embankment centerline. The findings indicate that the strength properties (φ,c) of the embankment fill have a crucial impact in promoting soil arching, leading to an increased load transfer to the piles in the middle and on the sides. Figure 8 demonstrates that the load efficiency changes at an accelerated rate when the cohesion of fill is less than 6 kN/m^2.

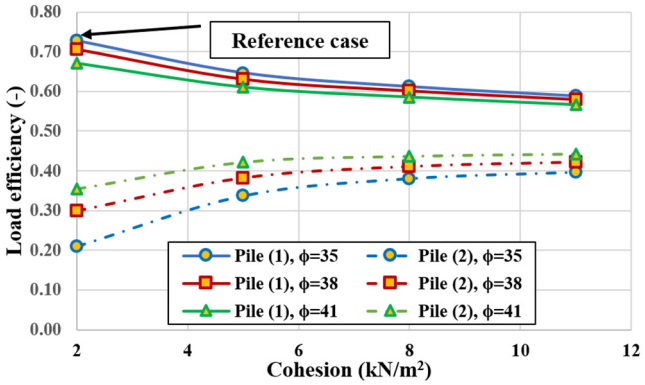


Figure 8. Influence of the cohesion and internal friction angle on the load efficiency.

To conduct a more in-depth examination of the embankment fill properties, Figure 9 presents an analysis of the influence of Young's modulus of the embankment soil with low cohesion (c = 2 kN/m^2) on load efficiency. The findings demonstrate that the load efficiency of pile 1 increases slightly and linearly with the Young's modulus, while the load efficiency of pile 2 remains relatively constant across the range of examined Young's moduli. These findings suggest that the stiffness of the soil has a slightly positive effect on promoting soil arching, which contributes to the enhancement of the load efficiency of pile 1.

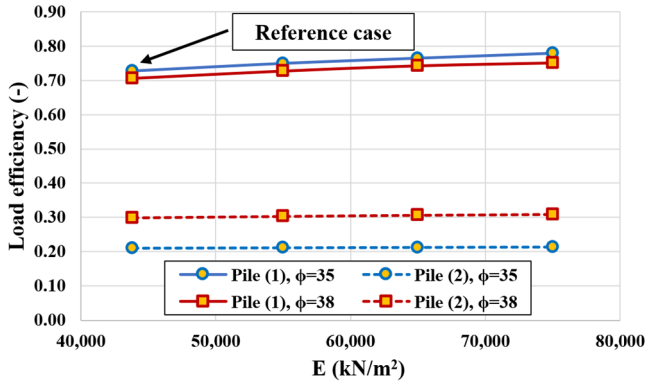


Figure 9. Influence of Young's modulus on the load efficiency.

The settlements of both the soil and the pile at the embankment base have been observed. Figure 10 summarizes the maximum settlement at the base of the embankment for different values of the cohesion and the internal friction angle. It appears that the maximum settlement decreases at an accelerated rate when the cohesion ranges between (2 and 5) kPa, particularly with (φ = 35). After that, the decrease becomes slight, as shown in Figure 10. Using soil with higher values of both cohesion and internal friction angle contributes to a reduction in the measured maximum settlement at the base of the embankment by 46% and 37%, respectively, compared to the reference case. This finding is in alignment with the outcomes documented by Xu et al. [16]. The decrease in settlement can be ascribed to the strength properties of the embankment fill, which promote an even distribution of the applied load within the embankment and improve the soil arching. This, in turn, leads to greater load transfer to all piles in the system. Consequently, the vertical load applied to the loose sand and geotextile reinforcement decreases, leading to a decrease in the maximum settlement. Regarding the influence of the elastic modulus of embankment fill, Figure 9 demonstrates the low effect of this parameter on the load efficiency. In other words, the increase of the elastic modulus has a small influence on the reduction of the settlements.

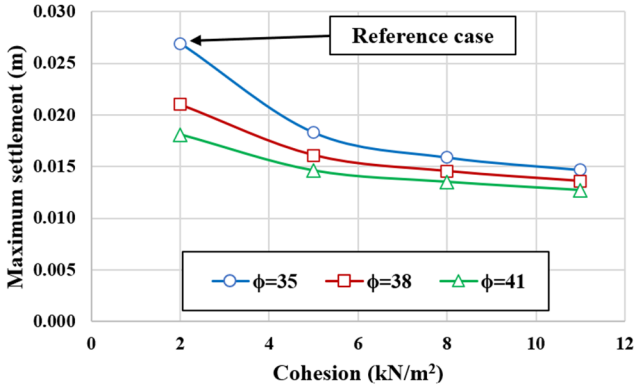


Figure 10. Influence of cohesion and internal friction angle on the maximum settlement.

Similarly, Figure 11 illustrates the differential settlement at the base of the embankment. The strength parameters of cohesion and internal friction angle have been found to result in a reduction of 48% and 50% in differential settlements, respectively. As previously discussed, the improved cohesion and internal friction angle contribute to a more equitable distribution of the applied vertical load and enhance the efficiency of the entire system, resulting in a reduction of the differential settlements.

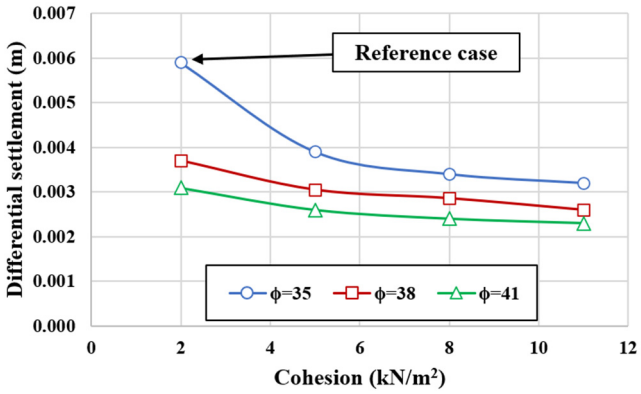


Figure 11. Influence of cohesion and internal friction angle on the differential settlement.

4.2. Influence of Horizontal Reinforcement

To investigate the impact of horizontal reinforcement on load distribution and settlement behavior, four scenarios were proposed, including the use of two layers of geotextile, full-folded geotextile layers, one geotextile layer (reference case), and one geocell, as depicted in Figure 12. For a more detailed explanation of the horizontal reinforcement scenarios, the following is provided: (1) two layers of geotextile, optimally positioned at 10 mm and 60 mm above the level of pile heads, which resulted in lower maximum settlement values according to this study; (2) a full-folded geotextile layer with a thickness of 15 mm, considered optimal compared to folded layers with thicknesses of 0 and 25 mm; (3) the reference case; and (4) an actual shape of geocell is utilized in this analysis. Hegde and Sitharam [31] and Yang et al. [32] performed experimental studies and compared the load-settlement behavior of the geocell with that of the corresponding simulated models to prove the competence of Plaxis 3D in the simulation of the geocell. Autodesk AutoCAD 2021 program was used to build the surface of the geocell, which was afterwards imported into Plaxis 3D. Extrude object tool was used to provide the geocell its required height. The dimensions are 15, 20, and 24 mm, which represent the cell height and size, respectively [33].

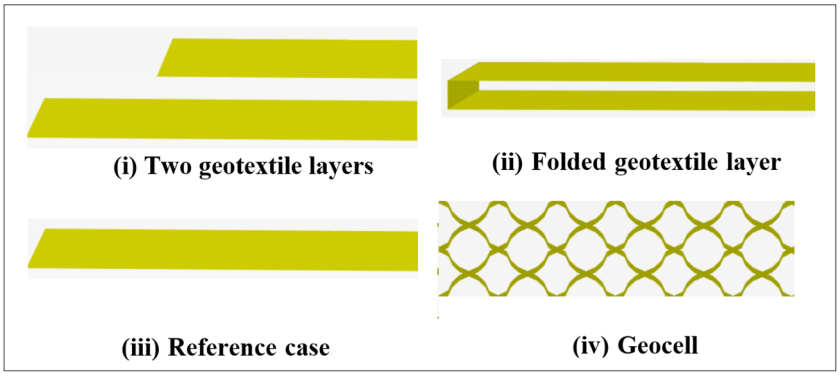


Figure 12. Different scenarios of horizontal reinforcement.

Figure 13 depicts the load efficiency distribution of piles (1, 2) for horizontal reinforcement scenarios. The findings indicate that the use of two layers of geotextile, with positions of 10 mm and 60 mm over the pile heads, was the most effective scenario, resulting in minimal variance in load efficiency between the two piles tested. This outcome was attributed to the improvement in load distribution. The utilization of a full-folded layer of geotextile also showed promising results, reducing the variance of load efficiency. On the other hand, the use of the geocell was found to be the least effective scenario, producing the worst results in comparison to the reference case.

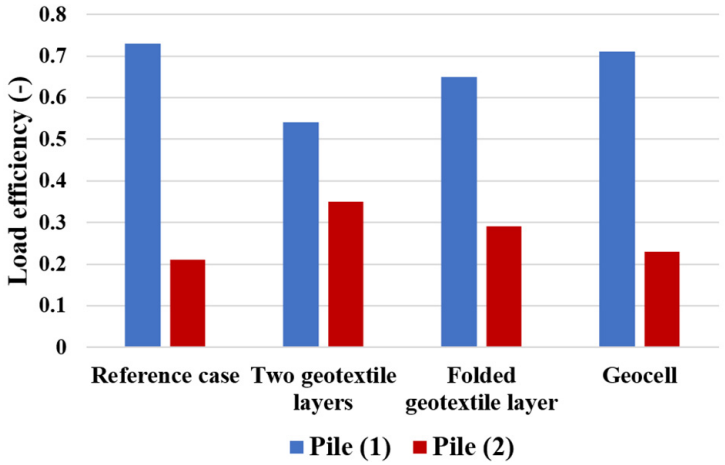


Figure 13. Influence of geosynthetic reinforcement on the load efficiency.

Figure 14 displays the load-settlement responses of different scenarios of horizontal reinforcement at the embankment base. It can be observed that in the scenario of geocell inclusion, the maximum settlements are slightly higher than those of the reference case. This can be explained by the inability of geocell reinforcement to retain the embankment fill over it because of the large size of cells, which leads, in turn, to further settlement of the soil. The inclusion of two geotextile layers exhibits more superior settlement behavior than the reference case, as shown in Figure 14. This is in line with the pertinent load efficiency findings when the optimum positions of the geotextile layers are taken into consideration. As can be seen, the maximum settlement in this scenario is around 30% lower than it was in the reference case.

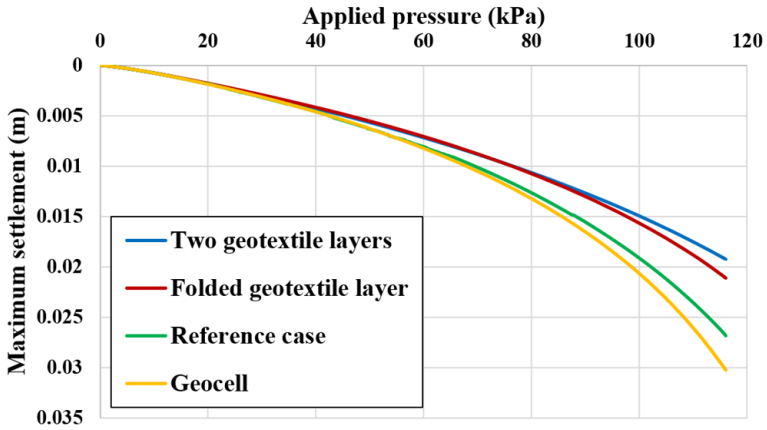


Figure 14. Influence of geosynthetic reinforcement on the maximum settlement.

4.3. Influence of the Pile Cap Shape

This study examined the impact of the shape of the pile cap on load efficiency and settlements at the foundation of the embankment. Three distinct shapes of the pile cap were considered, including a plus-shaped configuration (with a ratio of b = 2a), a square shape, and a circular shape (see Figure 15). The pile diameter was held constant at 0.027 m, while the area of the pile cap was varied. The comparison was conducted for the three shapes with the same area. In these analyses, four areas were considered: $A_{pile\ cap}$ = 2.0, 3.0, 4.0, and 5.0 A_{pile}, where $A_{pile\ cap}$ and A_{pile} denote the area of the pile cap and the cross-sectional area of the pile, respectively.

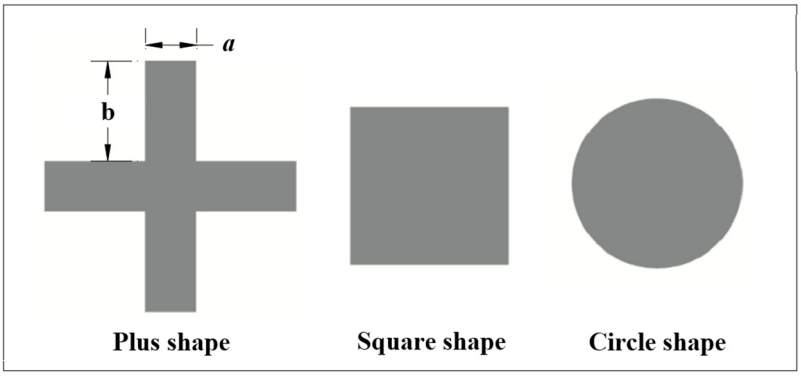


Figure 15. Different shapes of the pile cap for the same area.

The effectiveness of pile cap shapes in influencing the load efficiency of piles is evident in Figure 16, which illustrates how the shape of the pile cap directly impacts the load efficiency of the pile. The results of this study reveal that for small areas ($A_{pile\ cap}$ = 2.0, 3.0 A_{pile}), the use of a plus-shaped cap yields a higher load efficiency than that of a squared cap. On the other hand, using a circular cap results in the lowest load efficiency. As the area of the squared and circular pile caps increases, the load efficiency of squared and circular caps tends to remain constant. This can be attributed to the pile cap capacity to act as a shallow foundation and distribute a portion of the load to the soil underneath the cap, subsequently reducing the load on the pile head. Based on the results shown in Figure 16, the performance of both square and circular caps is comparable in terms of load efficiency.

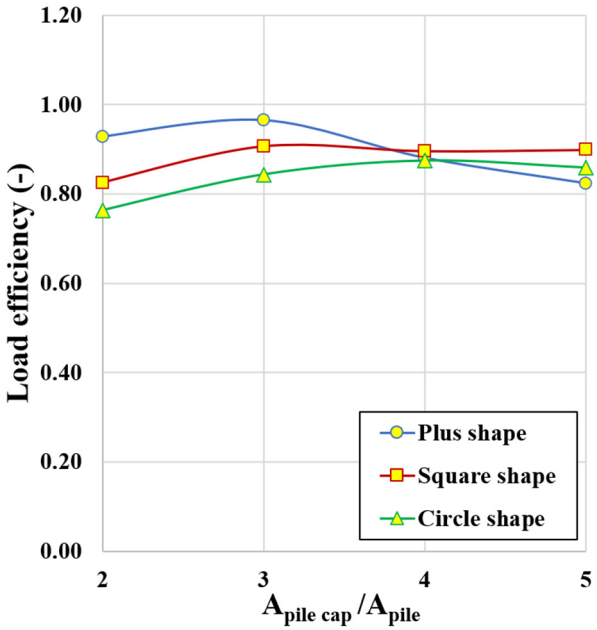


Figure 16. Influence of pile cap shape on the behavior of load efficiency.

The findings clearly demonstrate that adopting a plus-shaped cap completely alters the load efficiency behavior. The load efficiency increases as the pile cap area is enlarged, up to the value of ($A_{pile\ cap}$ = 3.0, A_{pile}) to reach the highest load efficiency, as shown in Figure 16. After that, it starts to decline with larger pile cap areas. The observed behavior can be explained by the blocking phenomenon, where the soil confined between the adjacent pile cap edges behaves as a part of these caps and moves downward upon loading as a single unit.

Figure 17 depicts the settlements (s_s, s_p) at the base of the embankment for various ratios of Apile cap/Apile, where s_s, s_p denote the maximum settlements of soil and pile,

respectively. For squared and circle shapes, the settlements decrease considerably with the enlargement of the pile cap area. Moreover, the space between the dashed and solid curves represents the differential settlements, while the results demonstrate that the differential settlements decrease gradually with larger cap areas. Generally speaking, the square shape seems to show a better behavior with regard to the maximum and differential settlements.

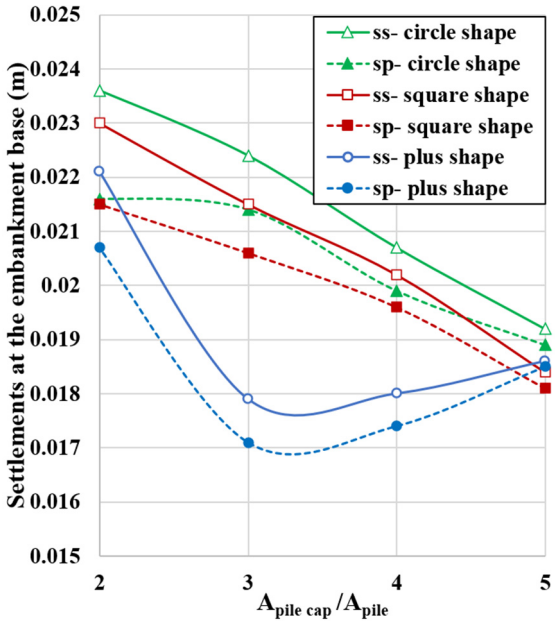


Figure 17. Influence of pile cap shape on the maximum and differential settlements.

In the case of plus shapes, the maximum settlements (s_s, s_p) decrease obviously until Apile cap/Apile reaches 3.0. Beyond that, the maximum settlements start to increase with larger areas of pile cap. Pertaining to the differential settlements, the reduction continues with the enlargement of the pile cap area, as shown in Figure 17. This can be attributed to the blocking phenomenon since the authors found a similar behavior of the neighboring pile caps to that of shallow foundations. For further explanation, Terzaghi et al. [34] proposed that the space between neighboring footings should range between (3 and 5) * B to behave as a single footing and prevent the interaction of the footings on each other; B denotes to the footing width. Moreover, Stuart [35] found that the settlements of two neighboring footings increase as the distance between them decreases. Furthermore, the findings by Alnmr and Alsirawan [36] illustrate that the shallow foundations with plus shape behave better with regard to the load-displacement in comparison with other shapes.

4.4. Influence of Pile Length (L), Pile Diameter (d), and Cap Width (a)

To assess the impact of pile length, diameter, and cap width on the distribution of axial forces and settlement behavior, this study uses the volume of the pile as a constant while comparing the influence of the aforementioned variables. Three distinct scenarios are considered to represent an increase in pile volume:

- Case A: the volume is increased by utilizing a square-shaped cap with a thickness of 20 mm, while maintaining constant values for pile length (400 mm) and diameter (27 mm).
- Case B: the volume is boosted by increasing the diameter of the pile while keeping the length constant at 400 mm (without cap).
- Case C: The volume is increased by raising the length of the pile while keeping the diameter constant at 27 mm (without cap). Table 2 illustrates the changes of volume based on pile length and the corresponding parameters.

Table 2. Changes of pile length, pile diameter, and pile cap width under the same volume.

Pile Length (m)	Volume (m^3)	Corresponding Pile Diameter (m)	Corresponding Cap Width (m)
0.4	0.000229	0.0270	0.0270
0.45	0.000258	0.0286	0.038
0.5	0.000286	0.0301	0.053
0.55	0.000315	0.0317	0.066
0.6	0.000344	0.033	0.076
0.7	0.0004	0.0357	-
d = 27 mm, no cap		L = 400 mm, no cap	L = 400 mm, d = 27 mm

Figure 18 illustrates how axial forces are distributed in the pile for a constant volume of 0.000344 m^3 in the three scenarios discussed above. It is observed that for a capped pile (case A), the axial force increases significantly along the pile cap thickness due to the concentration of force at the pile head and the negative skin friction at the upper part of the pile. Then, it gradually decreases along the pile due to the positive friction between the pile and surrounding soil. Similar behavior is observed in cases B and C, where the axial force increases as a result of negative skin friction between the pile and subsoil. Subsequently, it starts to decrease due to positive skin friction and tip resistance of the pile. The Figure 18 also demonstrates that the maximum axial forces are observed in case C, indicating that a growth in pile length under the same volume leads to transferring a larger part of the load to the soil beneath the pile, thus reducing settlements of the embankment.

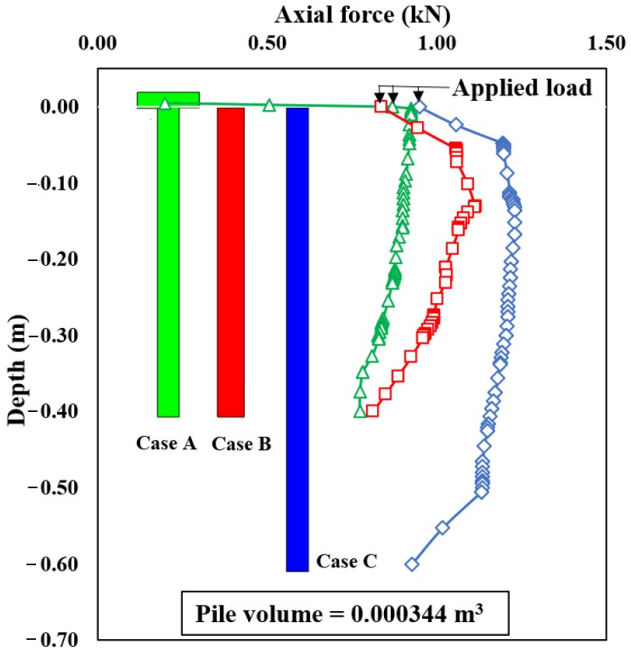


Figure 18. Axial forces along different types of pile.

According to the findings of the research conducted by Alsirawan and Koch [21] on GRPS embankment over soft soil, the addition of caps assists in increasing the amount of load transfer to the piles. Figure 18 indicates that the applied load in case C is greater than in case A, which contradicts the prior findings. For more clarification, Figure 19 illustrates the applied load at the pile heads (1, 2) for three scenarios, A, B, and C. The employment of capped piles supports the further distribution of the applied load over the piles of this system, which undoubtedly leads to a reduction in the amount of load applied in the piles in the centerline of the embankment.

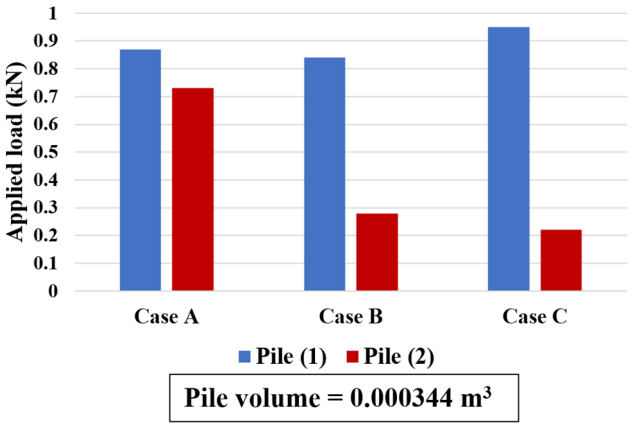


Figure 19. Applied load for different types of pile.

The maximum settlements at the base of the embankment for cases A, B, and C are shown in Figure 20. In case A, there is a significant reduction in maximum settlement as the pile cap area is increased to a corresponding volume of 0.000286 m^3, with only a slight decrease in settlement observed at higher cap area values. Case B demonstrates that the maximum settlement progressively decreases as the frictional area of the pile increases, in conjunction with an increase in pile volume. In case C, even though the frictional area of the pile remains constant, longer piles exhibit better behavior in terms of maximum settlement relative to case B. This can be attributed to an increased depth of subsoil improvement. These results align with those of Jamsawang et al. [37].

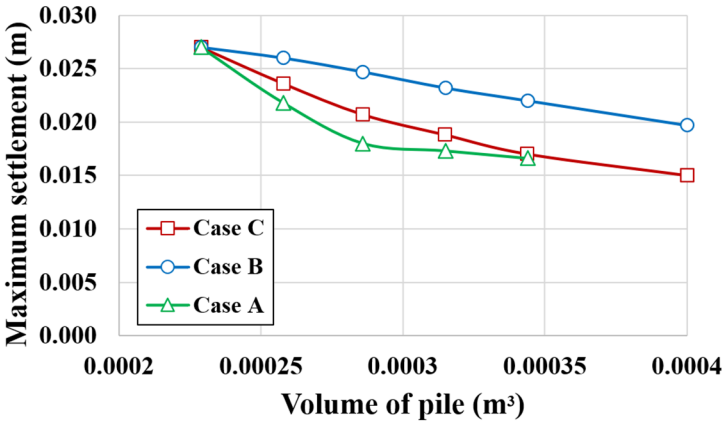


Figure 20. Maximum settlements for different types of pile.

Capped piles are commonly considered to be an optimal solution for reducing maximum settlement due to their ability to distribute the applied loads effectively.

The correlation between the pile shape and differential settlements is illustrated in Figure 21. As depicted in case A, a notable reduction in differential settlements is observed with an increase in the pile cap area. This trend indicates that the effect of pile cap area on differential settlements is significant until a threshold volume of 0.000286 m^3 is reached, beyond which the effect becomes negligible. For case B, the augmentation in the cross-sectional area of the pile results in a gradual and moderate reduction of differential settlements, in comparison to a substantial decrease observed in case A. Although the effect of the cross-sectional area on the differential settlements is not as pronounced as that of the pile cap area, it is still noteworthy that it plays a contributory role in the reduction of these settlements. For case C, which contained a boost of the length of the piles in a GRPS embankment, the differential settlement does not seem to have changed. This suggests that while extending the pile length can improve the overall stiffness of the embankment

system, it may not always have a remarkable impact on the differential settlement, as in the above case.

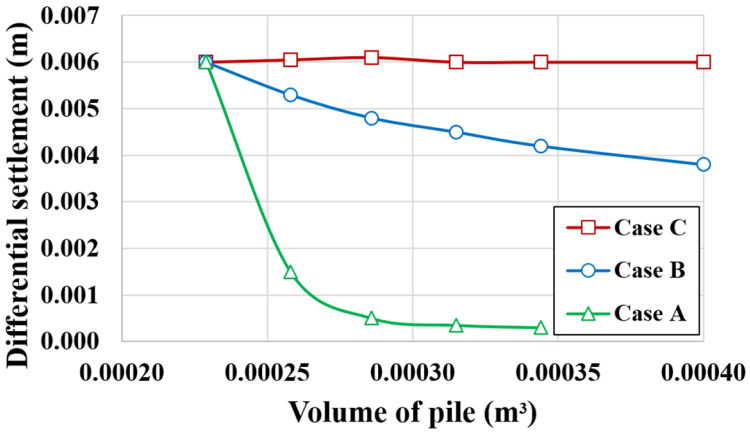


Figure 21. Differential settlements for different types of pile.

5. Conclusions

This study employed the construction of a laboratory-scale model to examine the performance of GRPS embankments over loose sandy soil. Subsequently, a numerical validated model was used to analyze the impact of different parameters, such as properties of embankment fill, horizontal reinforcement scenarios, pile cap shape, and pile type. This study aimed to achieve a more uniform distribution of the load over all piles of the system by analyzing the behavior of the GRPS embankment under various scenarios.

Based on the results of the laboratory model and the subsequent numerical investigation, several conclusions can be drawn from the findings of this study:

- The embankment fill properties—internal friction angle and cohesion—contribute to the promotion of the soil-arching phenomenon, leading to an increased load transmit to the piles in the middle and on the sides under the embankment, while the impact of the elastic modulus is considered low.
- The use of embankment fill with higher values for the internal friction angle and cohesion leads to a notable decrease of 46% and 37%, respectively, in maximum settlements at the base of the embankment. Moreover, this enhancement contributes to a reduction of 48% and 50%, respectively, in differential settlements.
- The use of two layers of geotextile with optimal positions over the pile heads can improve load distribution and reduce variance in load efficiency between the piles, and consequently, lead to a 30% decrease in maximum settlements at the base of the embankment.
- The load efficiency of a pile and the settlement of an embankment are directly influenced by the shape of the pile cap. In particular, a plus-shaped pile cap provides higher load efficiency for smaller areas, and the area of the pile cap is equal to three times that of the pile. Thereafter, this advantage diminishes as the pile cap area becomes larger. Conversely, squared and circular pile caps tend to function as shallow foundations, providing greater load efficiency for larger pile cap areas.
- The use of a plus-shaped pile cap can result in a significant reduction of maximum settlements, especially when the pile cap area is smaller. On the other hand, squared and circular pile caps exhibit similar settlement behavior. Additionally, the utilization of pile caps can significantly reduce differential settlements when compared to other parameters.
- Extending the pile length leads to a greater transfer of the load to the soil below. However, the use of capped piles contributes to further distribution of the load over the piles in the middle and on the sides.

➢ Employing longer piles and capped piles results in a considerable reduction of maximum settlements. Moreover, capped piles significantly contribute to decreasing differential settlements.

In summary, the practical implications derived from this research equip engineers with actionable insights to optimize the design and construction of geosynthetic-reinforced piled embankments on loose sandy soil. These findings offer a valuable toolbox for addressing load distribution, settlement control, and overall stability, further advancing the field of geotechnical engineering and its ability to create enduring embankment structures.

As part of future endeavors, it is recommended that subsequent research delve into the intricate interplay between the properties inherent to sandy soils and their potential ramifications on the behavior of GRPS embankments. Investigating these nuanced interactions will undoubtedly enrich our understanding and inform refined methodologies, thus contributing to the ongoing refinement and evolution of geotechnical engineering practices.

Author Contributions: Conceptualization, R.A. and A.A.; methodology, R.A.; software, R.A.; validation, R.A. and A.A.; formal analysis, R.A.; investigation, R.A.; writing—original draft preparation, R.A.; writing—review and editing, R.A.; supervision, E.K. All authors have read and agreed to the published version of the manuscript.

Funding: This work was funded by Széchenyi István University.

Data Availability Statement: Data will be made available upon request.

Conflicts of Interest: The authors declare no conflict of interest.

References

1. Raja, M.N.A.; Shukla, S.K. Ultimate bearing capacity of strip footing resting on soil bed strengthened by wraparound geosynthetic reinforcement technique. *Geotext. Geomembr.* **2020**, *48*, 867–874. [CrossRef]
2. Raja, M.N.A.; Shukla, S.K. Experimental study on repeatedly loaded foundation soil strengthened by wraparound geosynthetic reinforcement technique. *J. Rock Mech. Geotech. Eng.* **2021**, *13*, 899–911. [CrossRef]
3. Deb, K.; Sivakugan, N.; Chandra, S.; Basudhar, P.K. Generalized Model for Geosynthetic-Reinforced Granular Fill-Soft Soil with Stone Columns. *Int. J. Geomech.* **2007**, *7*, 266–276. [CrossRef]
4. Han, J.; Gabr, M.A. Numerical Analysis of Geosynthetic-Reinforced and Pile-Supported Earth Platforms over Soft Soil. *J. Geotech. Geoenviron. Eng.* **2002**, *128*, 44–53. [CrossRef]
5. Hewlett, W.; Randolph, M. Analysis of piled embankments. *Ground Eng.* **1988**, *22*, 12–18.
6. Kempfert, H.; Gobel, C.; Alexiew, D.; Heitz, C. German recommendations for the reinforced embankments on pile-similar elements. In *Geosynthetics in Civil and Environmental Engineering*; Springer: Berlin/Heidelberg, Germany, 2004; pp. 697–702. [CrossRef]
7. Abusharar, S.; Zheng, J.; Chen, B.; Yin, J. A simplified method for analysis of a piled embankment reinforced with geosynthetics. *Geotext. Geomembr. J.* **2009**, *27*, 39–52. [CrossRef]
8. *BS 8006*; Code of Practice for Strengthened Reinforced Soils and Other Fills. BSI: London, UK, 2010. Available online: http://worldcat.org/isbn/0580242161 (accessed on 24 August 2023).
9. EBGEO. *Recommendations for Design and Analysis of Earth Structures Using Geosynthetic Reinforcements*; German Geotechnical Society: Essen, Germany, 2011.
10. Van Eekelen, S.; Bezuijen, A.; VanTol, A. An analytical model for arching in piled embankments. *Geotext. Geomembr.* **2013**, *39*, 78–102. [CrossRef]
11. Pham, T. Analysis of geosynthetic-reinforced pile-supported embankment with soil-structure interaction models. *Comput. Geotech.* **2020**, *121*, 103438. [CrossRef]
12. Alsirawan, R.; Koch, E.; Alnmr, A. Proposed Method for the Design of Geosynthetic-Reinforced Pile-Supported (GRPS) Embankments. *Sustainability* **2023**, *15*, 6196. [CrossRef]
13. Nuñez, M.; Dias, D.; Kastner, R.; Poilpré, C. Soft Ground Improved by Rigid Vertical Piles. Experimental and Numerical Study of Two Real Cases in France. In Proceedings of the International Conference on Case Histories in Geotechnical Engineering, Arlington, VA, USA, 11–16 August 2008; Missouri University of Science and Technology: Rolla, MO, USA, 2008.
14. Chevalier, B.; Villard, P.; Combe, G. Investigation of Load Transfer Mechanisms in Geotechnical Earth Structures with Thin Fill Platforms Reinforced by Rigid Inclusions. *Int. J. Geomech.* **2010**, *11*, 239–250. [CrossRef]
15. Van Eekelen, S.; Bezuijen, A.; Lodder, H.; Van Tol, A. Model experiments on piled embankments. Part I. *Geotext. Geomembr.* **2012**, *32*, 69–81. [CrossRef]
16. Xu, C.; Song, S.; Han, J. Scaled model tests on influence factors of full geosynthetic-reinforced pile-supported embankments. *Geosynth. Int.* **2016**, *23*, 140–153. [CrossRef]

17. Pham, T.; Dias, D. 3D numerical study of the performance of geosynthetic-reinforced and pile-supported embankments. *Soils Found.* **2021**, *61*, 1319–1342. [CrossRef]
18. Briançon, L.; Simon, B. Pile-supported embankment over soft soil. *Geosynth. Int.* **2017**, *24*, 293–305. [CrossRef]
19. Kerry Rowe, R.; Liu, K. Three-dimensional finite element modelling of a full-scale geosynthetic-reinforced, pile-supported embankment. *Can. Geotech. J.* **2015**, *52*, 2041–2054. [CrossRef]
20. Pham, T.; Tran, Q.A.; Villard, P.; Dias, D. Numerical Analysis of Geosynthetic-Reinforced and Pile-Supported Embankments Considering Integrated Soil-Structure Interactions. *Geotech. Geol. Eng.* **2023**, *24*, 1–22. [CrossRef]
21. Alsirawan, R.; Koch, E. Behavior of embankment supported by rigid inclusions under static loads-parametric study. In Proceedings of the 12th IEEE International Conference on Cognitive Infocommunications—CogInfoCom 2021, Online, 23–25 September 2021; pp. 385–389.
22. Hello, B.; Villard, P. Embankments reinforced by piles and geosynthetics—Numerical and experimental studies dealing with the transfer of load on the soil embankment. *Eng. Geol.* **2009**, *106*, 78–91. [CrossRef]
23. Zhang, Z.; Wang, M.; Ye, G.; Han, J. A novel 2D-3D conversion method for calculating maximum strain of geosynthetic reinforcement in pile-supported embankments. *Geotext. Geomembr.* **2019**, *47*, 336–351. [CrossRef]
24. Wang, T.; Nguyen, V.; Bui, P.; Luo, Q.; Liu, K.; Zhang, L. Three-dimensional physical modeling of load transfer in basal reinforced embankments under differential settlement. *Geotext. Geomembr.* **2023**, *51*, 330–341. [CrossRef]
25. Pongsivasathit, S.; Chai, J.; Bergado, D. Laboratory model test on the behavior of floating soil-cement column improved ground. In Proceedings of the 14th Asian Regional Conference on Soil Mechanics and Foundation Engineering, Hong Kong, China, 23–27 May 2011.
26. Cao, W.; Zheng, J.; ZhangRong-Jun Zhang, R.; Zhang, R. Field test of a geogrid-reinforced and floating pile-supported embankment. *Geosynth. Int.* **2016**, *23*, 348–361. [CrossRef]
27. Zhang, H.; Wang, H.; Li, X.; Li, W.; Wu, J.; Lv, C.; Song, X.; Liu, M. An Analysis of Floating Geogrid-Reinforced Pile-Supported Embankments Containing Deep Softened Soil. *Arab. J. Sci. Eng.* **2021**, *46*, 10855–10868. [CrossRef]
28. Shen, P.; Xu, C.; Han, J. Geosynthetic-reinforced pile-supported embankment: Settlement in different pile conditions. *Geosynth. Int.* **2021**, *27*, 315–331. [CrossRef]
29. Esmaeili, M.; Khajehei, H. Mechanical behavior of embankments overlying on loose subgrade stabilized by deep mixed columns. *J. Rock Mech. Geotech. Eng.* **2016**, *8*, 651–659. [CrossRef]
30. *EN ISO 14688-1*; Geotechnical Investigation and Testing—Dentification and Classification of Soil—Part 1: Identification and Description. International Organization for Standardization: Geneva, Switzerland, 2002.
31. Hegde, A.; Sitharam, T. 3-Dimensional numerical modelling of geocell reinforced sand beds. *Geotext. Geomembr.* **2015**, *43*, 171–181. [CrossRef]
32. Yang, X.; Han, J.; Parsons, R.; Leshchinsky, D. Three-dimensional numerical modeling of single geocell-reinforced sand. *Front. Architect. Civ. Eng.* **2010**, *4*, 233–240. [CrossRef]
33. Ari, A.; Misir, G. Three-dimensional numerical analysis of geocell reinforced shell foundations. *Geotext. Geomembr.* **2021**, *49*, 963–975. [CrossRef]
34. Terzaghi, K.; Peck, R.; Mesri, G. *Soil Mechanics in Engineering Practice*; John Wiley and Sons: New York, NY, USA, 1996.
35. Stuart, J. Interference Between Foundations, with Special Reference to Surface Footings in Sand. *Géotechnique* **1962**, *12*, 15–22. [CrossRef]
36. Alnmr, A.; Alsirawan, R. Numerical Study of the Effect of the Shape and Area of Shallow Foundations on the bearing Capacity of Sandy Soils. *Acta Polytech. Hung.* **2023**, *12*, 693.
37. Jamsawang, P.; Yoobanpot, N.; Thanasisathit, N.; Voottipruex, P.; Jongpradist, P. Three-dimensional numerical analysis of a DCM column-supported highway embankment. *Comput. Geotech.* **2016**, *72*, 42–56. [CrossRef]

Disclaimer/Publisher's Note: The statements, opinions and data contained in all publications are solely those of the individual author(s) and contributor(s) and not of MDPI and/or the editor(s). MDPI and/or the editor(s) disclaim responsibility for any injury to people or property resulting from any ideas, methods, instructions or products referred to in the content.